Angular differential cross sections for the excitation of 1^1S helium to the 2^1S and 2^1P states by 25- to 100-keV-proton impact

T. J. Kvale,* D. G. Seely, D. M. Blankenship, E. Redd, T. J. Gay,
M. Kimura,† E. Rille,‡ J. L. Peacher, and J. T. Park
Physics Department, University of Missouri—Rolla, Rolla, Missouri 65401-0249
(Received 30 January 1985)

Angular differential cross sections for the proton-impact excitation of ground-state helium (1^1S) to the 2^1S and 2^1P states have been measured for the first time in the energy range 25 to 100 keV with use of the energy-loss technique. The data indicate that, for very small scattering angles, at 25 keV the 2^1S differential cross section is greater than the 2^1P differential cross section. For impact energies greater than 50 keV, the 2^1P differential cross section clearly dominates over the 2^1S cross section in the very small scattering angle region. The present data have been numerically summed and integrated to compare with previous absolute experimental measurements on related processes. These are in very good agreement with the present results. An eight-state impact-parameter calculation incorporating the electron-capture channel was performed and resulted in the best agreement with the experimentally determined differential cross sections.

I. INTRODUCTION

The proton-helium collisional system provides an important opportunity for understanding the basic physics governing atomic collisions. This is the fundamental collisional system in the class of ion-two electron atom interactions, and because of its importance, numerous experimental[1–6] and theoretical[7–23] efforts have been devoted to studying excitation to the lowest excited states in this system. Recent studies on the related processes of elastic scattering[24] and electron capture[25] in proton-helium collisions have resulted in information about these processes that can be applied to the general theory of collisions. For instance, it was demonstrated by Peacher *et al.*[24] that no channel or process can be safely neglected in an accurate theory concerning the elastic scattering of protons from helium. Likewise, the excitation measurements on this system may help in understanding the general impact-excitation phenomena in ion-atom collisions.

The fact that the proton-helium system can be experimentally and theoretically handled with well-established techniques makes this system ideally suited to test basic concepts about collisional physics. The proton is a structureless projectile which does not complicate the understanding of the scattering. As predicted by the Wigner spin-conservation rule the triplet states are not significantly excited. This effect has been studied by van Eck *et al.*[26] (and references cited therein) at 30 keV. They reported that the triplet total cross sections by proton impact were at least a factor of 100 less than the corresponding total cross sections by hydrogen impact. The $n=2$ singlet states available for excitation from the ground 1^1S state are only the optically forbidden 2^1S and the optically allowed 2^1P states.

Although data for the composite $n=2$ level have existed for some time, it has been demonstrated in the literature[3,9–11] that the composite $n=2$ level results mask vast discrepancies in the individual state resolved 2^1S and 2^1P cross-section predictions. The poor agreement between the various theoretical predictions[7,9] as demonstrated in the literature indicate that those collisional processes are not well understood.

The processes that were studied in the present experiment are

$$\mathrm{H}^+ + \mathrm{He}(1^1S) \rightarrow \mathrm{H}^+(\theta) + \mathrm{He}^*(2^1S)$$
$$\rightarrow \mathrm{H}^+(\theta) + \mathrm{He}^*(2^1P) .$$

The data reported here represent the first measurements of angular differential cross sections for proton-impact excitation to these states in this fundamental collisional system.

II. EXPERIMENTAL METHOD

A. Apparatus

The University of Missouri—Rolla Ion-Energy-Loss Spectrometer (UMR-IELS), shown in Fig. 1, was the instrument that provided the necessary high resolution in both scattering angle and energy loss for measurements of differential cross sections for proton-impact excitation of helium to the 2^1S and 2^1P states. The UMR-IELS apparatus, data acquisition method, and method of deconvolution of the real differential cross sections from the apparent cross sections are described in detail in previous papers.[3,24,25,27–33] Only a synopsis of these aspects of the UMR-IELS will be presented here for continuity. The experimental arrangement was an acceleration-deceleration system so that the voltage fluctuations of the 15- to 200-kV high-voltage power supply did not degrade the energy-loss resolution. In this manner an $E/\Delta E$ of 10^5, or better, was achieved. The variable-angle ion accelerator was pivoted about the center of the scattering chamber by a computer-controlled stepping motor. The horizontal motion of the ion accelerator about the center of the

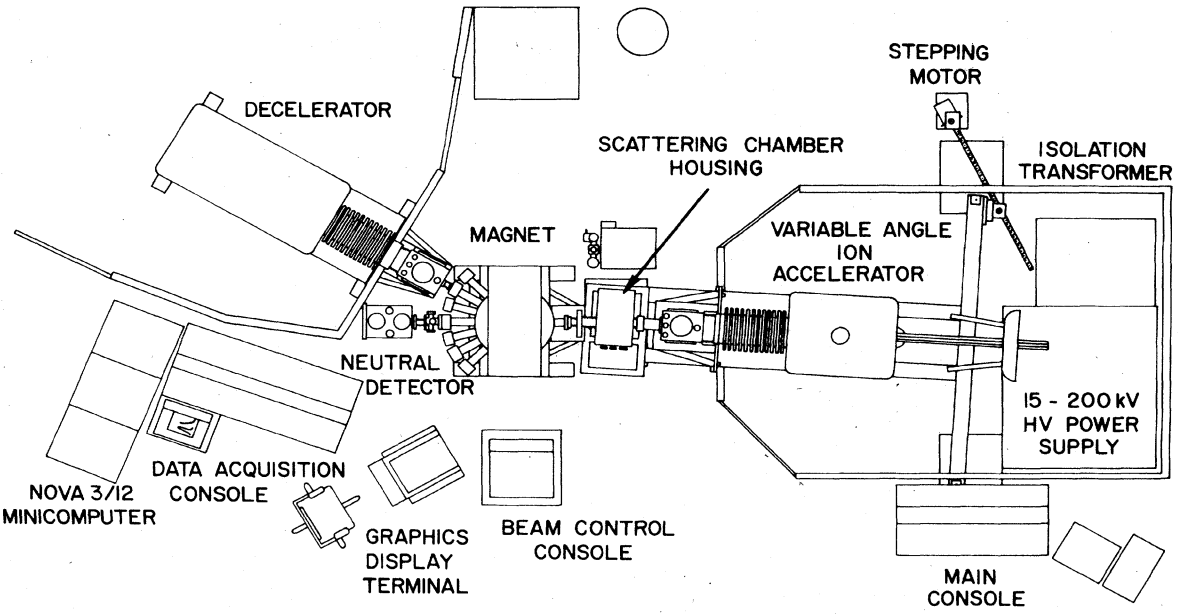

FIG. 1. Drawing of the University of Missouri—Rolla Ion-Energy-Loss Spectrometer (UMR-IELS). The unit chair located to the left of the graphics display terminal provides an estimation of the size of the UMR-IELS apparatus.

scattering chamber defined the scattering plane. The laboratory magnet and decelerator were stationary and determined the detection trajectory of the scattered ion beam.

Protons were produced by a Colutron ion source consisting of a plasma region, extractor-einzel lens, and Wien filter. The Wien filter selected the desired ion species and provided additional focusing of the ion beam. A set of deflection plates and a 0.102-cm aperture-movable flag assembly were added after the Wien filter for ion-beam diagnostics and spatial definition. The ion source typically produced a stable proton current of 1 to 10 nA measured in the movable flag.

A voltage, consisting of the voltage of the main high-voltage power supply and a precision energy-loss (ΔV) voltage, was applied to the accelerator terminal to accelerate the proton beam to the desired collisional energy. The spatial definition of the incident ion beam was provided by a set of horizontal and vertical movable slits, located between the deflection-plate assembly and the scattering chamber.

The scattering chamber was differentially pumped by a trapped 6-in. oil diffusion pump. The background pressure in the scattering chamber and housing, without target gas, was typically 5×10^{-8} Torr, and with 10 mTorr of helium in the chamber, the background pressure in the housing increased to 2×10^{-7} Torr. Helium gas was admitted to the chamber through a piezoelectric valve controlled by a microcomputer-based device.[34] The scattering-chamber pressure was measured by an MKS Instruments Model No. 170 capacitance manometer. A movable cup was located so that it could be inserted into the incident proton beam at the center of the scattering chamber. The current on the cup was independent of the scattering angle and provided normalization of the incident proton beam. The front and back apertures defined the scattering length ($l=1.14\pm0.02$ cm) in this experiment.

A laboratory magnet located after the scattering chamber provided a d.c. magnetic field perpendicular to the scattering detection plane. This arrangement permitted the positive identification of the scattered particles. Protons that had not undergone an electron-capture collision were directed through the 30° port of the magnet and into the deceleration column. Two sets of deflection plates prior to the deceleration column allowed the scattered ion beam to be directed into the hemispherical energy-analyzer system inside the decelerator terminal. Between the deflection-plate system and the deceleration column were movable slits which defined the detector solid angle.

The analyzer design was based on the hemispherical energy analyzer used by Kuyatt and Plummer[35] for their electron-impact field-emission studies. The hemispherical analyzer, Fig. 2, was designed with the help of Kuyatt[36] and modifications were kept to a minimum in order to make use of the significant amount of existing design calculations of the focal properties of the device.[35–39] The angular extent of the hemispheres was chosen to be 135° along the plane of the ion-beam trajectory. The hemispherical analyzing elements were constructed with a mean radius of 2.540 cm and a separation of 0.635 cm between the hemispheres. The ion optics elements in the hemispherical analyzer and in the zoom lens permitted the control of the kinetic energy of the protons entering the analyzing region, which for this experiment was less than 2 eV. A set of real apertures, which were located on the first element, created an image at the entrance of the hemispheres. This minimized the contribution of reflected ions from the detected signal. Because the object appeared as a virtual aperture, the energy resolution result-

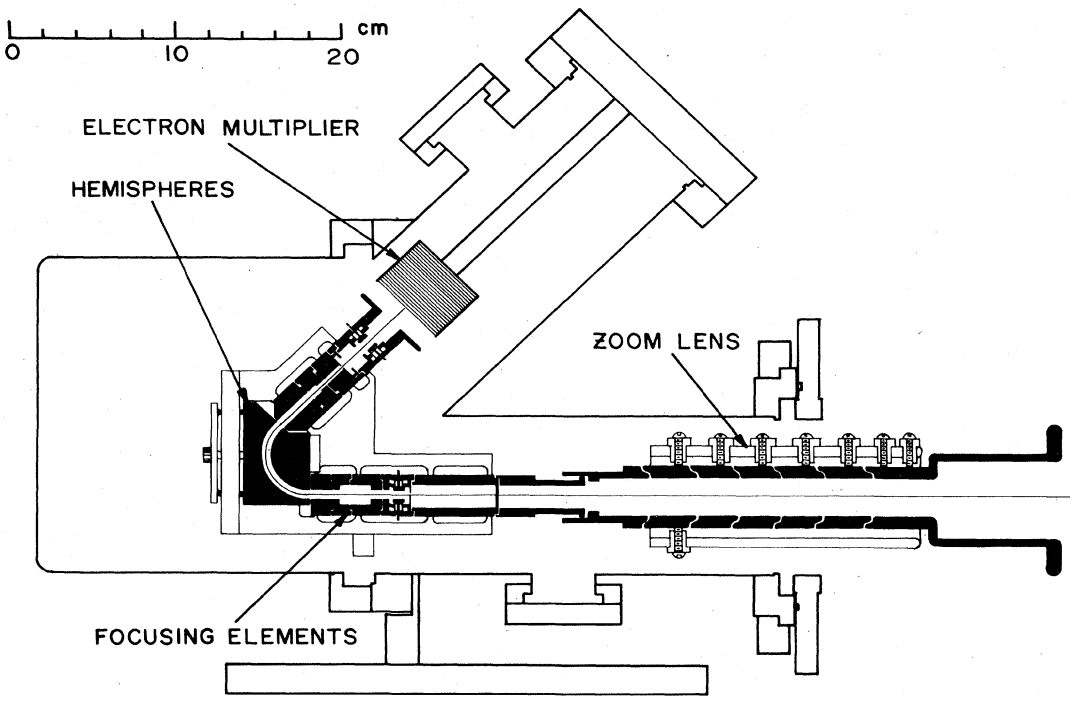

FIG. 2. Cross-sectional drawing of the hemispherical energy analyzer which is located inside the decelerator terminal.

ing from the image size was a function of the lens parameters. The operating values of the present analyzer are in agreement with the design values. Typically, the analyzer was operated with 0.64 V across the hemispheres. The energy resolution of the analyzer system was better than 0.4 eV.

A focused mesh electron multiplier detected the protons transmitted by the analyzer and was the first stage of amplification for the data signal. The count rates were low enough to permit pulse-counting techniques and thus the data were in digital form. Additional amplifiers, discriminators, and a high-speed decade divider shaped the digital signal before being transmitted over a quartz rod from the decelerator terminal at high voltage to the pulse counter in the data acquisition console at earth potential. A Data General NOVA 3/12 minicomputer recorded the data while controlling the scattering-chamber pressure, accelerator angle, and energy-loss voltage ΔV.

The difference in potential between the variable-angle ion accelerator and the decelerator ΔV is related to the energy lost by the ion during the collision and is referred to as the energy-loss voltage. The voltage on the decelerator was kept constant and, by varying the ion accelerator voltage, an energy-loss spectrum was obtained. When the energy-loss voltage corresponded to a collisional excitation energy of a state, a peak was detected in the proton count rate. Figure 3 shows typical energy-loss spectra acquired with the UMR-IELS at collisional energies of 25 and 100 keV. The zero energy-loss peak corresponds to both the unscattered incident proton beam and the elastically scattered protons. The first excitation peaks are at 20.62- and 21.22-eV energy loss,[40] which correspond to excitation of the 2^1S and 2^1P states, respectively.

B. Deconvolution techniques

Two deconvolution programs were employed to extract the real differential cross sections from the data. The angular deconvolution program is identical to that reported earlier[3,29,30] and will be discussed briefly in the following paragraphs. Before the data were entered into the angular deconvolution program, an energy-loss deconvolution program was used in order to subtract the contribution of current from adjacent state excitations adding to the detected current of the process being measured.

In order to accomplish this, the NOVA minicomputer was programmed to acquire the data in a multichannel scaler mode. Typically, data spectra were taken with 10 mTorr of helium in the scattering chamber and background spectra were taken with no gas in the scattering chamber. Each spectrum was pressure corrected and the possible variance in the scattering-chamber incident-proton current corrected before the spectra were input to the energy-loss deconvolution program. This procedure was repeated for each scattering angle.

The energy-loss deconvolution was performed in a manner similar to that used to deconvolute total cross sections reported earlier.[27,28] Modifications to that program allowed for the entire angular set of energy-loss spectra to be processed initially to correct for the kinematic-energy-loss shift in the spectra prior to the energy-loss deconvolu-

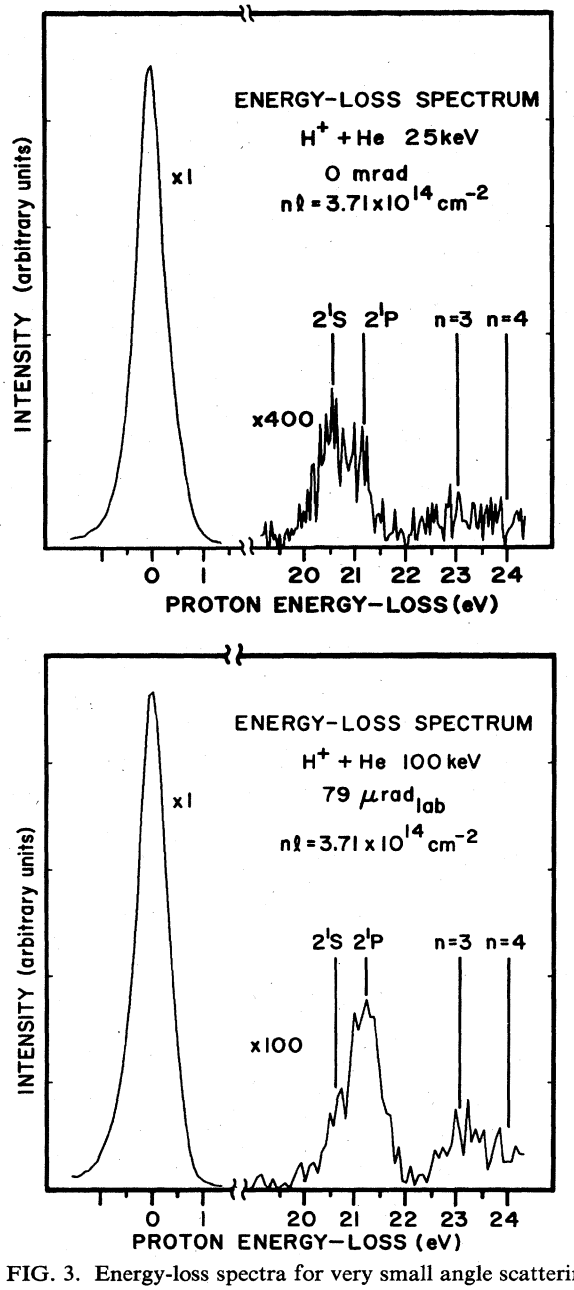

FIG. 3. Energy-loss spectra for very small angle scattering of protons by helium at 25- and 100-keV$_{lab}$. Notice the change in relative magnitudes of the 2^1S and 2^1P at the two energies.

tion of the states. The data with helium in the scattering chamber were corrected for instrument-caused-background noise and then normalized to the incident-proton current measured in the scattering-chamber cup. Background data, with the scattering chamber evacuated, were also corrected for instrument-caused-background noise and scaled to account for charge-changing collisions.[41–43] Subtraction of the corrected background data from the corrected data resulted in the data which underwent the energy-loss deconvolution. In the energy-loss deconvolution program, the incident-proton energy distribution at zero scattering angle is assumed to represent the apparatus energy resolution function $\Phi(\xi)$. In the equations, θ is the scattering angle in the laboratory frame and ξ is the energy-loss value which has been defined so that $\xi=0$ corresponds to the peak of the elastically scattered beam. The measured energy-loss spectrum $dR(\theta,\xi)/d\xi$ is a convolution of the apparatus energy-loss resolution function $\Phi(\xi)$ with the actual energy-loss distribution $dI(\theta,\xi)/d\xi$;

$$\frac{dR(\theta,\xi)}{d\xi}=\int \frac{dI(\theta,\xi')}{d\xi'}\Phi(\xi'-\xi)d\xi' .$$

The measured current is a sum of the convoluted excitations located at the proper energy-loss values.

The individual discrete state excitations are taken to be count rates times δ functions in energy loss at the energy values of the various states. The ionization is assumed to follow a ξ^{-3} dependence.[28] The assumed distribution is then a sum over all discrete and continuum states;

$$\frac{dI(\theta,\xi)}{d\xi}=\sum_q\{I_q(\theta)\delta[\xi-(e_q+\xi_k)]\}+A(\theta)\xi^{-3} ,$$

where $dI(\theta,\xi)/d\xi$ is the assumed energy-loss distribution at a particular scattering angle θ, e_q is the excitation energy in eV of the qth atomic state, ξ_k is the kinematic energy loss due to conservation of energy and momentum, $I_q(\theta)$ is the magnitude of the contribution atomic state q has in comprising the energy-loss spectrum, $A(\theta)$ is the coefficient of the ionization term. If ξ is less than the first ionization threshold 24.59 eV, then $A(\theta)$ is set to zero.

A least-squares fit was made to the measured spectrum $dR(\theta,\xi)/d\xi$ using the assumed distribution $dI(\theta,\xi)/d\xi$ convoluted with the incident-beam distribution. The general method of a least-squares fit of the data with functions is given in McCalla.[44] Thus one defines

$$D(\theta)=\sum_i\left[\frac{dR(\theta,\xi_i)}{d\xi_i}-\int\frac{dI(\theta,\xi')}{d\xi'}\Phi(\xi'-\xi_i)d\xi'\right]^2 ,$$

where ξ_i is the particular measured energy-loss location, and the sum is over all energy-loss locations. By minimizing $D(\theta)$ at each scattering angle, the individual state count rates $I_q(\theta)$ were obtained.

In general, the higher states made only a small correction to the results for the 2^1S and 2^1P states because the $n=2$ states are well separated from the rest of the spectrum as can be seen in Fig. 3. The $I_q(\theta)$ for $q=2^1S$ and 2^1P obtained from the energy-loss deconvolution were used in the angular deconvolution program to obtain the experimentally determined differential cross sections that are reported in this paper.

The values returned from the energy-loss deconvolution program resulted in apparent differential cross sections

$$\frac{ds_q}{d\Omega}=\frac{I_q(\theta)}{I_0 nl\,\Delta\Omega} , \tag{1}$$

where $I_q(\theta)$ is the count rate returned from the energy-loss deconvolution program at the scattering angle θ due to the qth process, I_0 is the total current at zero energy loss integrated over the scattering angle, n is the helium-

TABLE I. Proton-impact excitation of helium to the 2^1S, 2^1P, and the composite $n=2$ level at 25 to 100 keV.

Angle ($mrad_{c.m.}$)	$(d\sigma/d\Omega)_{2^1S}$ ($cm^2/sr_{c.m.}$)	$(d\sigma/d\Omega)_{2^1P}$ ($cm^2/sr_{c.m.}$)	Composite $n=2$ ($cm^2/sr_{c.m.}$)
	(25-keV)$_{lab}$ differential cross sections		
0.00	$(1.07\pm0.52)\times10^{-11}$	$(7.22\pm4.29)\times10^{-12}$	$(1.79\pm0.85)\times10^{-11}$
0.10	$(8.14\pm2.61)\times10^{-12}$	$(4.23\pm3.61)\times10^{-12}$	$(1.24\pm0.51)\times10^{-11}$
0.21	$(5.14\pm1.14)\times10^{-12}$	$(1.92\pm0.89)\times10^{-12}$	$(7.06\pm1.40)\times10^{-12}$
0.31	$(4.07\pm0.95)\times10^{-12}$	$(1.49\pm0.51)\times10^{-12}$	$(5.40\pm0.86)\times10^{-12}$
0.41	$(2.46\pm0.89)\times10^{-12}$	$(9.02\pm4.40)\times10^{-13}$	$(3.25\pm1.18)\times10^{-12}$
0.52	$(1.82\pm0.93)\times10^{-12}$	$(6.83\pm2.78)\times10^{-13}$	$(2.51\pm0.82)\times10^{-12}$
0.73	$(8.12\pm0.20)\times10^{-13}$	$(1.80\pm0.49)\times10^{-13}$	$(9.92\pm0.69)\times10^{-13}$
0.82	$(5.09\pm0.67)\times10^{-13}$	$(1.27\pm0.68)\times10^{-13}$	$(6.36\pm1.42)\times10^{-13}$
0.94	$(2.44\pm0.73)\times10^{-13}$	$(1.50\pm0.37)\times10^{-13}$	$(3.94\pm1.10)\times10^{-13}$
1.04	$(7.93\pm7.95)\times10^{-14}$	$(1.43\pm0.65)\times10^{-13}$	$(2.22\pm0.14)\times10^{-13}$
1.36	$(3.07\pm2.02)\times10^{-14}$	$(5.28\pm1.82)\times10^{-14}$	$(8.35\pm0.26)\times10^{-14}$
$\sigma_{tot}(cm^2)$	$(3.80\pm1.30)\times10^{-18}$	$(1.51\pm0.82)\times10^{-18}$	$(5.31\pm1.80)\times10^{-18}$
	(50-keV)$_{lab}$ differential cross sections		
0.00	$(5.14\pm1.19)\times10^{-11}$	$(5.81\pm4.12)\times10^{-11}$	$(1.10\pm0.46)\times10^{-10}$
0.08	$(3.46\pm0.59)\times10^{-11}$	$(3.46\pm1.99)\times10^{-11}$	$(6.92\pm2.31)\times10^{-11}$
0.17	$(2.09\pm0.39)\times10^{-11}$	$(2.13\pm1.04)\times10^{-11}$	$(4.22\pm1.17)\times10^{-11}$
0.30	$(7.72\pm2.46)\times10^{-12}$	$(8.89\pm5.60)\times10^{-12}$	$(1.66\pm0.80)\times10^{-11}$
0.42	$(3.75\pm2.71)\times10^{-12}$	$(3.75\pm1.42)\times10^{-12}$	$(7.50\pm2.75)\times10^{-12}$
0.50	$(1.65\pm0.94)\times10^{-12}$	$(2.02\pm1.33)\times10^{-12}$	$(3.67\pm2.13)\times10^{-12}$
0.54	$(1.54\pm1.42)\times10^{-12}$	$(1.81\pm1.59)\times10^{-12}$	$(3.35\pm2.90)\times10^{-12}$
$\sigma_{tot}(cm^2)$	$(6.85\pm1.03)\times10^{-18}$	$(7.80\pm3.00)\times10^{-18}$	$(1.47\pm0.38)\times10^{-17}$
	(75-keV)$_{lab}$ differential cross sections		
0.00	$(2.75\pm0.34)\times10^{-11}$	$(1.04\pm0.89)\times10^{-10}$	$(1.32\pm0.11)\times10^{-10}$
0.05	$(2.12\pm0.36)\times10^{-11}$	$(7.67\pm0.86)\times10^{-11}$	$(9.79\pm1.10)\times10^{-11}$
0.15	$(1.26\pm0.40)\times10^{-11}$	$(2.81\pm0.57)\times10^{-11}$	$(4.07\pm0.70)\times10^{-11}$
0.25	$(1.04\pm0.55)\times10^{-11}$	$(1.56\pm0.27)\times10^{-11}$	$(2.60\pm0.65)\times10^{-11}$
0.36	$(3.08\pm0.72)\times10^{-12}$	$(6.62\pm2.68)\times10^{-12}$	$(9.70\pm3.30)\times10^{-12}$
0.55	$(3.88\pm2.02)\times10^{-13}$	$(1.16\pm0.92)\times10^{-12}$	$(1.55\pm1.09)\times10^{-12}$
0.66	$(2.37\pm1.90)\times10^{-13}$	$(2.73\pm1.52)\times10^{-13}$	$(5.10\pm2.47)\times10^{-13}$
0.77	$(1.94\pm1.01)\times10^{-13}$	$(1.74\pm0.69)\times10^{-13}$	$(3.68\pm1.68)\times10^{-13}$
0.97	$(1.73\pm1.91)\times10^{-13}$	$(8.14\pm2.05)\times10^{-14}$	$(2.54\pm2.01)\times10^{-13}$
1.07	$(8.43\pm7.34)\times10^{-14}$	$(4.68\pm1.34)\times10^{-14}$	$(1.31\pm0.87)\times10^{-13}$
$\sigma_{tot}(cm^2)$	$(4.73\pm0.69)\times10^{-18}$	$(9.64\pm0.92)\times10^{-18}$	$(1.44\pm0.12)\times10^{-17}$
	(100 keV)$_{lab}$ differential cross sections		
0.00	$(8.97\pm6.98)\times10^{-11}$	$(1.85\pm0.99)\times10^{-10}$	$(2.74\pm1.01)\times10^{-10}$
0.03	$(7.27\pm5.37)\times10^{-11}$	$(1.55\pm0.68)\times10^{-10}$	$(2.27\pm0.72\times10^{-10}$
0.14	$(2.58\pm1.74)\times10^{-11}$	$(6.71\pm2.24)\times10^{-11}$	$(9.30\pm3.59)\times10^{-11}$
0.24	$(9.22\pm5.81)\times10^{-12}$	$(2.33\pm1.57)\times10^{-11}$	$(3.27\pm1.78)\times10^{-11}$
0.38	$(2.71\pm2.10)\times10^{-12}$	$(6.49\pm3.35)\times10^{-12}$	$(9.21\pm4.65)\times10^{-12}$
0.45	$(1.55\pm1.60)\times10^{-12}$	$(2.45\pm2.10)\times10^{-12}$	$(3.99\pm3.46)\times10^{-12}$
0.58	$(5.02\pm6.28)\times10^{-13}$	$(7.30\pm6.40)\times10^{-13}$	$(1.24\pm1.25)\times10^{-12}$
0.66	$(3.86\pm3.93)\times10^{-13}$	$(3.42\pm3.67)\times10^{-13}$	$(7.26\pm7.35)\times10^{-13}$
0.83	$(4.46\pm4.06)\times10^{-13}$	$(7.32\pm9.81)\times10^{-13}$	$(1.18\pm1.39)\times10^{-12}$
$\sigma_{tot}(cm^2)$	$(5.36\pm2.43)\times10^{-18}$	$(1.37\pm0.55)\times10^{-17}$	$(1.91\pm0.71)\times10^{-17}$

target number density, l is the scattering-chamber length, and $\Delta\Omega$ is the solid angle subtended by the detector. The apparent differential cross section is related to the actual differential cross section by

$$\frac{ds_q}{d\Omega}=\frac{1}{\Delta x\,\Delta y}\int_{\Delta x}dx\int_{\Delta y}dy\int d\Omega'\frac{1}{I_0}\frac{dI}{d\Omega'}\frac{d\sigma_q}{d\Omega}\ ,$$

where Δx and Δy are the width and height of the detector window, Ω' represents the direction of the incident ion beam, and $dI/d\Omega$ is the angular distribution of the incident ion beam. In order to obtain the actual differential cross section from the apparent differential cross section we take

$$\frac{d\sigma_q}{d\Omega}(\theta)=f(\theta)\frac{ds_q}{d\Omega}(\theta)\ ,$$

where $f(\theta)$ is a slowly varying apparatus-beam function of θ only and can be represented by a truncated Taylor-series expansion. In this way the actual differential cross section is deconvoluted from the apparent differential cross section by the angular deconvolution program. The mathematics and a more detailed description of the method are given in Ref. 3.

III. DATA AND RESULTS

The results of this investigation represent the first measurements of angular differential cross sections for the excitation of the two singlet states in the $n=2$ manifold of helium by proton impact in the 25- to 100-keV energy region. The present measurements are absolute and do not depend on other experiments or theories in the determination of the magnitude or shape of the cross sections. The reported differential cross sections are the averaged results from individual angular-sequence measurements described earlier. A typical angular sequence required $\sim$7 h to complete. Table I reports the numerical values of the various measured angular differential cross sections and integrated total cross sections at 25-, 50-, 75-, and 100-keV impact energies. The uncertainties quoted are one standard deviation from the averaged results. The 25- and 100-keV angular differential cross sections are also shown in Figs. 4 and 5, along with the theoretical calculations. In some cases, the error bars are smaller than the graphed data-point symbol.

The errors in the absolute magnitudes of the differential cross sections were determined by the uncertainties inherent in the measurements of the apparent differential cross sections given in Eq. (1). These were $I_q(\theta)-(\pm5\%)$; $I_0-(<\pm0.1\%)$; $n-(\pm2.5\%)$; $l-(\pm1.8\%)$; and $\Delta\Omega-(\pm5\%)$. This results in the uncertainty in the absolute magnitude of the differential cross sections to be $\pm7.7\%$. This uncertainty affected the 2^1S and 2^1P cross sections in a similar manner. Other errors or uncertainties included collisional energy $-(\pm3\%)$; energy-loss scale $-(\pm0.1\%)$; and the angular position $-(\pm19\ \mu\text{rad}_{\text{lab}})$.

The 2^1S and 2^1P total cross sections were obtained by numerically integrating the present differential cross sections according to the equation

$$\sigma_{\text{tot}}=2\pi\int_0^{\theta_{\max}}\frac{d\sigma}{d\Omega}\sin\theta\,d\theta\ , \qquad (2)$$

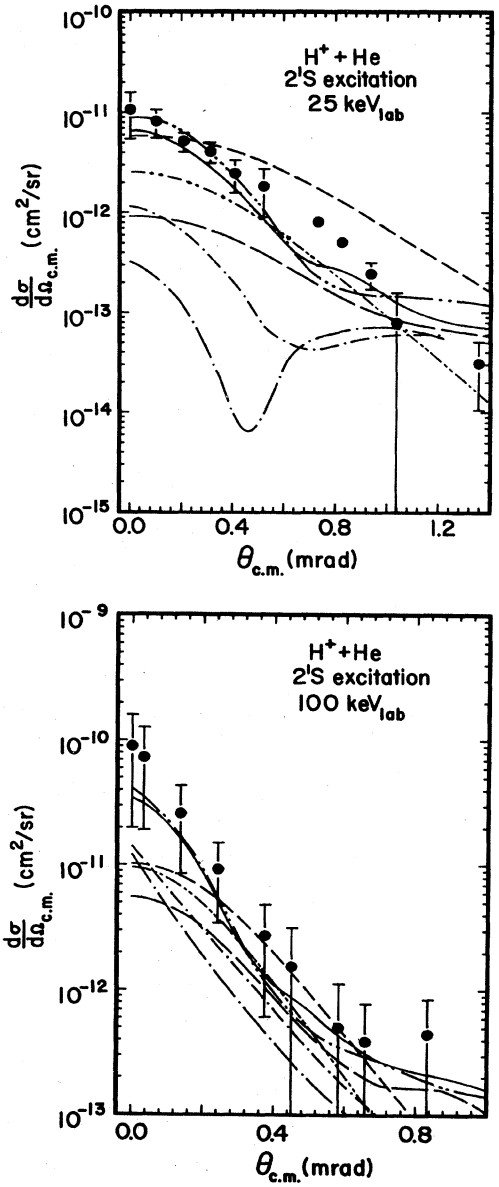

FIG. 4. Angular differential cross sections for the 2^1S excitation of helium by 25- and 100-keV$_{\text{lab}}$-proton impact. The circles are data from the present work. The error bars represent one standard deviation in the averaged, deconvoluted data (see text). The theoretical calculations are B1, short dash, Ref. 7; ESA, solid curve, present work; FSA, long dash dot dot, Ref. 7; GA2, long dash dot, Ref. 9; SSG, short dash dot, Ref. 9; TSA, long dash, Ref. 7; and VPSA, short dash dot dot, Ref. 10.

where $\theta_{\max}$ is the largest scattering angle for which data were acquired. There was a concern that the measured angular data went to large enough angles to provide an accurate total cross section. Therefore, the contribution to the total cross section for protons scattered at angles greater than $\theta_{\max}$ was estimated by a linear extrapolation. The extrapolated data amounted to a negligible fraction of the integrated total cross section over the actual data points.

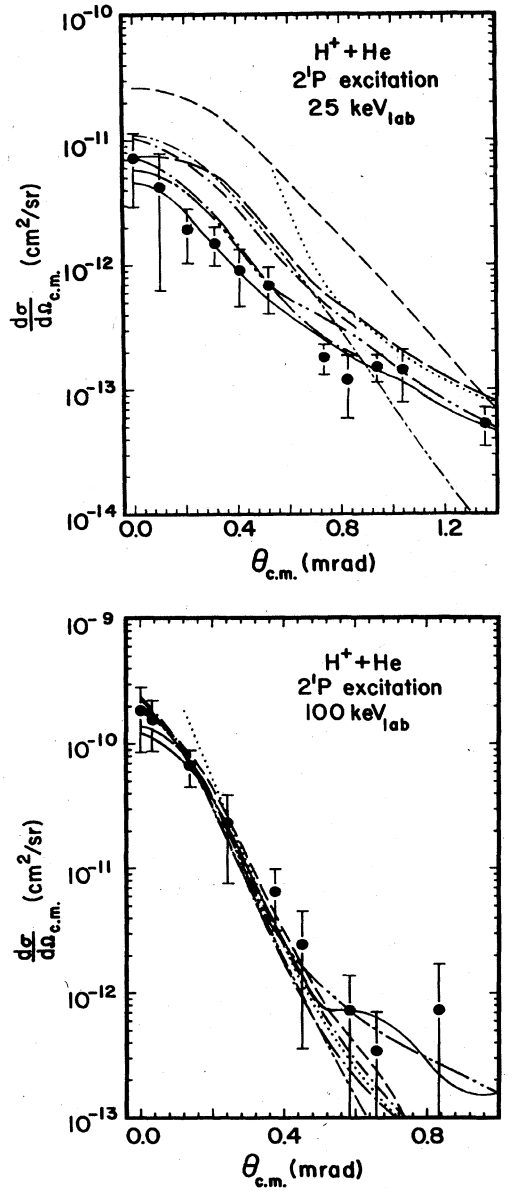

FIG. 5. Angular differential cross sections for the 2^1P excitation of helium by 25- and 100-keV$_{lab}$-proton impact. The symbols are the same as described in Fig. 4, with the addition of GA1 (dot dot, Ref. 8).

IV. DISCUSSION

A. Experimental studies

Although the present results are the first measurements of angular differential cross sections for the excitation of helium to the 2^1S and 2^1P states by proton impact, related measurements have been performed for this system. Previous measurements for excitation to the first excited states from the ground state in this system were for either total cross sections[1,2,4] or angular differential cross sections for excitation to the composite $n=2$ level, summed over the individual $n=2$ states.[3]

The differential cross sections measured by the energy-loss technique of the present work were numerically integrated according to Eq. (2) to obtain total cross sections. Previously measured total cross sections include the work of Park and Schowengerdt[1,2] for proton-impact excitation of helium to the $n=2$ states in the 25- to 125-keV impact-energy region using the energy-loss technique, and the work of Hippler and Schartner[4] using the optical technique for the 2^1P, 3^1P, and 4^1P total cross sections in the 150- to 1000-keV impact-energy region. The present data are in good agreement with the previous results, except at 25 keV where the present results indicate that the 2^1S total cross section is greater than the 2^1P total cross section. However, at 25 keV our results lie within the error bars of the previous measurements.

While the various theoretical approximation techniques generally agree in their predictions of the total cross sections, their different physical assumptions may result in quantitatively different predictions of the corresponding angular differential cross sections. Thus a more stringent test of the theoretical models is effected by comparing them with experimental cross sections which are differential in angle. The first measurements of angular differential cross sections for proton-impact excitation of helium to the $n=2$ levels were published in 1978 by Park *et al.*[3] The energy and angular ranges of those measurements were similar to that of the present data. In 1981, improvements to the apparatus extended the angular range of the measurements to, in some cases, over 3 mrad in the center-of-mass system.[45]

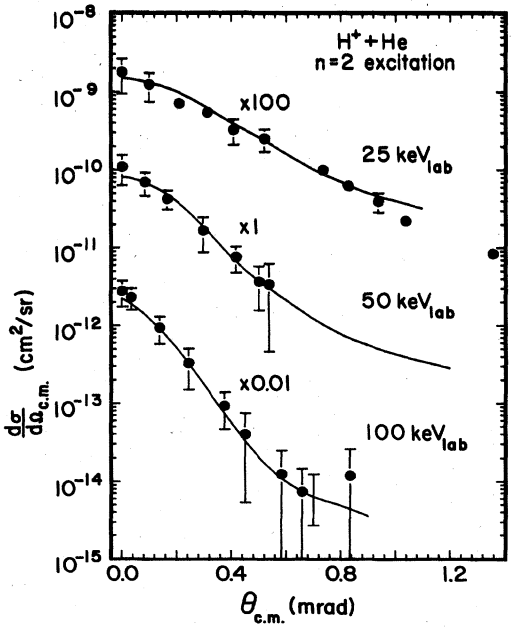

FIG. 6. Experimentally determined composite $n=2$ angular differential cross sections for proton-impact excitation of helium at 25-, 50-, and 100-keV$_{lab}$. The 25- and 100-keV cross sections have been multiplied by 100 and 0.01, respectively, for clarity. The circles are data of the present work and the solid lines are absolute measurements from Ref. 3. For small scattering angles, the error bars are comparable in both works.

By adding together the individual differential cross sections of the present work, a comparison with previous results[3,45] is made. As shown in Fig. 6, the 1978 measurements are in excellent agreement with the present differential cross sections. The experimental technique in both cases was an energy-loss technique; however, the data acquisition and apparatus differed significantly between the former and present measurements. The agreement of the present data with the previously reported composite $n=2$ angular differential cross sections and the previous individual 2^1S and 2^1P total cross sections indicates the accuracy of the three absolute, independent measurements. With this three-way agreement between the measurements, definitive statements about the scattering processes are now possible.

B. Previous theoretical calculations

State-resolved angular differential cross-section determinations are very sensitive to the approximations employed. For the proton-helium system there exist several calculations in various theoretical frameworks highlighting different physical processes of the collision. In general, the agreement of the theoretical calculations with the experimentally measured cross sections improves with increasing impact energy. This is consistent with the approximations inherent in the calculations. The 2^1P differential cross section was accurately predicted at all energies by three different theoretical calculations, whereas for the 2^1S excitation, agreement of the calculations with our data was limited to the impact energy of 100 keV. Even at this energy, the calculations generally underestimated the differential cross section.

In 1974, Flannery and McCann[7] reported theoretical calculations of the angular differential excitation cross sections for proton-helium scattering at intermediate energies. They presented the first Born (B1) approximation and the results of a two-state approximation (TSA) and a four-state approximation (FSA) which were based on the multistate impact-parameter approximation (MSIPA). The first Born approximation ignores the dynamics of the collision; thus it simplifies the collisional system to the point that detailed information of the system is lacking. This reduces its usefulness to that of a reference calculation which provides at best moderately accurate results for intermediate energy collisions.

The other two calculations reported in Ref. 7 were conducted in the MSIPA. In the TSA the initial helium state $(1s^2)\ 1^1S$ and the particular final helium state $(1s2s)\ 2^1S$ or $(1s2p_0)\ 2^1P$ and $(1s2p_{\pm1})\ 2^1P$ are employed to calculate the differential cross sections. By limiting the sum over the states to the initial and final states, only the direct excitation channel was included and all other couplings were omitted. This resulted in the small angle scattering having an angular dependence similar to B1, which includes only direct excitation.

The four-state approximation (FSA) includes the $(1s^2)\ 1^1S$, the $(1s2s)\ 2^1S$, the $(1s2p_0)\ 2^1P$, and the $(1s2p_{\pm1})\ 2^1P$ states for calculating the differential cross sections. By expanding the sum in the MSIPA to include all $n=2$ singlet states, the FSA accounted for direct excitation as well as the coupling between the 2^1S and 2^1P states. The FSA resulted in angular differential cross sections which were in generally good agreement with our data as shown in Figs. 4 and 5. The difference between the FSA and the TSA at small angles is due to the long-range $2s$-$2p$ coupling, which is not taken into account in the B1 or TSA.

There have been two differential cross-section calculations performed in the Glauber approximation for excitation in the proton-helium system. Chan and Chang[8] employed the Glauber approximation (GA1) for calculating the 2^1P cross section at 25-, 100-, and 1000-keV impact energies. The differential cross sections were reported as functions of momentum transfer. The small-angle approximation was employed to convert momentum transfer to scattering angle. The GA1 results appear to "blow up" as the scattering angle goes to 0 mrad.

Sur *et al.*[9] have also presented results for a full Glauber approximation (GA2) and for a single scattering Glauber approximation (SSG). The SSG approximation neglects the double-scattering term in the full Glauber amplitude. These results are shown in Figs. 4 and 5. In the 2^1P case the GA2 and SSG results are similar. However, the GA2 results provide the best agreement with our data. At 100 keV the GA1, GA2, and SSG results are all falling off faster than our data at the largest scattering angles measured. In the 2^1S case the GA2 and SSG results are in poor agreement with our experimental results at 25 keV. At 100 keV the curve shapes are in better agreement, but the magnitudes of the angular differential cross sections are less than our data.

Theodosiou[10] applied the Vainshtein-Presnyakov-Sobelman approximation (VPSA) to this system in 1981 to obtain the differential cross sections at 25-, 50-, and 100-keV impact energies. Essentially, the VPSA is an improvement of the Born approximation. The scattering event is assumed to be due to interaction between the proton projectile and the active electron. This interaction is treated exactly. The VPSA accounts for the distortion of the atomic system by the Coulombic field of the proton by also examining the projectile-target core interaction. The wave functions are also required to have the correct asymptotic form.[10,46] This results in a differential cross section which has a factor multiplying the differential cross section obtained from the first Born approximation. The factor is a complicated function of the momentum transfer and is less than one.

For the 2^1S case (see Fig. 4) the VPSA results are too low near 0 mrad and at the larger scattering angles they are falling too rapidly. For the 2^1P case (see Fig. 5) the VPSA results at 25 keV are too high near 0 mrad. The results at 100 keV represent the data well, as do the other calculations, for the very small scattering angles near 0 mrad. However, again at the larger scattering angles the VPSA results fall too rapidly.

C. Eight-state approximation

The inclusion of additional states to account for electron capture have been suggested[16,18] as possible improvements to the FSA. This would include the additional cou-

plings that are thought to affect excitation to the $n=2$ states of helium. At 25-keV impact energy, the electron-capture cross section to all bound atomic-hydrogen states is an order of magnitude larger than the $n=2$ excitation cross section.[3,25] The electron capture into the $2p$ state of atomic hydrogen is very close in energy with the excitation of the 2^1P states of helium according to the molecular correlation diagram. This is a long-range effect, so the small angle scattering into the 2^1S and 2^1P states should be affected.

To investigate this coupling, we have performed an eight-state approximation (ESA) calculation in the MSIPA framework. The method used a two-center atomic-orbital (TCAO) expansion which included electron translation factors (ETF's).[47,48] The ESA calculation employed hydrogenic wave functions for the $1s$, $2s$, $2p_0$, and $2p_{\pm1}$ states of hydrogen and the $1s$ state of the He^+ ion as well as the $(1s^2)\ 1^1S$, $(1s2s)\ 2^1S$, $(1s2p_0)\ 2^1P$, and $(1s2p_{\pm1})\ 2^1P$ states of helium. The wave functions used for the helium atom were those employed by Flannery and McCann.[7] The results of this calculation are shown in Figs. 4 and 5. One of the overall effects of including the electron-capture channels into the MSIPA calculation was to decrease the magnitudes of the differential cross section for excitation to both the 2^1S and the 2^1P states at lower energies. The agreement of our ESA calculation with our data is generally very good. The 2^1P differential cross sections were accurately predicted by our ESA over the present energy region 25 to 100 keV. At the higher energies, both our ESA and the FSA calculations predicted a similar angular dependence of the differential cross sections. This is consistent with the fact that the magnitude of the electron-capture cross section is decreasing at the higher impact energies.

Another effect of including the electron-capture channel into the calculation was to smooth out the structure in the 25-keV, 2^1S differential cross-section prediction of the FSA calculation. Compared with the FSA prediction, our ESA resulted in better agreement of the predicted differential cross section with our data at angles greater than ~ 0.6 mrad in the center of mass. There appears to be an observed increase in the agreement of the predictions with the data as more states are included in the MSIPA.

V. CONCLUSION

The data presented in this paper are the first measurements of cross sections for the excitation to the 2^1S and 2^1P states of helium by proton impact as a function of scattering angle. The angular range of our measurements was limited to the very small angle scattering region, which is important in determining the total cross section. The present measurements are absolute. They are in good agreement with the previous measurements of either the composite $n=2$ angular differential cross sections or the total cross sections of the individual state excitations.

The theories were in general agreement with our data for the differential cross sections for the optically allowed 2^1P excitation and were in poorer agreement with the optically forbidden 2^1S excitation. One conclusion that was made from studying the multistate-impact-parameter approximations and our data is that the coupling between the various states during the collision is important in the excitation of the $n=2$ states of helium. The poorer agreement of the theories with the data for 25-keV impact energy may indicate that additional state couplings would more accurately describe the scattering at the lower impact energies. This was observed in the improved agreement of our ESA calculation over the TSA calculation with our data.

The Glauber approximations systematically underestimated the 2^1S differential cross sections, yet agreed fairly well with the 2^1P differential cross sections. However, the agreement of the GA2 2^1P calculations with the data may be fortuitous because the inclusion of the double-scattering term resulted in worse agreement with the 2^1S differential cross sections.

This effort has demonstrated the importance of state-resolved angular differential cross sections in the proton-helium scattering system. This system can be probed at a deeper level because the 2^1P cross section is a composite of the different $m_L=0$ and $m_L\pm1$ sublevel cross sections of that state. By performing coincidence measurements between the scattered protons which have excited the 2^1P state and the 58.4-nm 2^1P-1^1S photons, these cross sections can be obtained.

ACKNOWLEDGMENTS

This work was funded by a grant from the National Science Foundation, No. NSF-PHY-81-06050. The eight-state approximation (ESA) calculation was funded by a grant from the U.S. Department of Energy, No. DOE-DE-FG02-84ER53175. One of us, T.J.K., wants to thank the staff at the Oak Ridge National Laboratory for their assistance.

*Present address: Oak Ridge National Laboratory, P. O. Box X, Oak Ridge, TN 37831.

†Present address: Joint Institute for Laboratory Astrophysics, National Bureau of Standards and University of Colorado, P. O. Box 440, Boulder, CO 80309.

‡Present address: Kastenlangen 63, A-6850 Dornbirn, Austria.

[1]J. T. Park and F. D. Schowengerdt, Phys. Rev. **185**, 152 (1969).

[2]F. D. Schowengerdt, Ph.D. dissertation, University of Missouri—Rolla, 1969.

[3]J. T. Park, J. M. George, J. L. Peacher, and J. E. Aldag, Phys. Rev. A **18**, 48 (1978).

[4]R. Hippler and K. H. Schartner, J. Phys. B **7**, 618 (1974).

[5]M. Abignoi, M. Barat, J. Baudon, J. Fayeton, and J. C. Houver, J. Phys. B **5**, 1533 (1972).

[6]C. Bernes, *Abstracts of Contributed Papers,* in *Proceedings of XIII International Conference on the Physics of Electronic and Atomic Collisions, Berlin, 1983,* edited by J. Eickler, W. Fritsch, I. V. Hertel, N. Stolterfoht, and U. Wille (North-Holland, Amsterdam, 1983).

[7]M. R. Flannery and K. J. McCann, J. Phys. B **7**, 1558 (1974).

[8]F. T. Chan and C. H. Chang, Phys. Rev. A **11**, 1097 (1975).
[9]S. K. Sur, Shyamal Datta, and S. C. Mukherjee, Phys. Rev. A **24**, 2465 (1981).
[10]Constantine E. Theodosiou, Phys. Lett. **83A**, 254 (1981); the 2^1S and 2^1P differential cross sections were made available to us by private communication.
[11]Shyamal Datta, C. R. Mandal, and S. C. Mukherjee, J. Phys. B **13**, 4791 (1980).
[12]R. J. Bell, Proc. Phys. Soc. London **78**, 903 (1961).
[13]K. L. Bell, D. J. Kennedy, and A. E. Kingston, J. Phys. B **1**, 218 (1968); **1**, 1037 (1968).
[14]J. van den Bos, Phys. Rev. **181**, 191 (1969).
[15]J. van den Bos, Physica (Utrecht) **42**, 245 (1969).
[16]M. R. Flannery, J. Phys. B **3**, 306 (1970).
[17]A. R. Holt, J. Hunt, and B. L. Moiseiwitsch, J. Phys. B **4**, 1318 (1971).
[18]S. Begun, B. H. Bransden, and J. Coleman, J. Phys. B **6**, 837 (1973).
[19]D. Baye and P. H. Heenen, J. Phys. B **6**, 1255 (1973).
[20]K. Roy and S. C. Mukherjee, Phys. Lett. **44A**, 147 (1973).
[21]Charles J. Joachain and Robert Vanderpoorten, J. Phys. B **7**, 817 (1974).
[22]G. J. Seddon and K. E. Barnard, J. Phys. B **7**, 2476 (1974).
[23]S. K. Sur and S. C. Mukherjee, Phys. Rev. A **19**, 1048 (1979); Shyamal Datta, S. K. Sur, and S. C. Mukherjee, *ibid.* **25**, 3422 (1982).
[24]J. L. Peacher, T. J. Kvale, E. Redd, P. J. Martin, D. M. Blankenship, E. Rille, V. C. Sutcliffe, and J. T. Park, Phys. Rev. A **26**, 2476 (1982).
[25]P. J. Martin, K. Arnett, D. M. Blankenship, T. J. Kvale, J. L. Peacher, E. Redd, V. C. Sutcliffe, J. T. Park, C. D. Lin, and J. M. McGuire, Phys. Rev. A **23**, 2858 (1981).
[26]J. van Eck, F. J. de Heer, and J. Kistenmaker, Physica (Utrecht) **30**, 1171 (1964).
[27]J. T. Park, J. E. Aldag, J. M. George, and J. L. Peacher, Phys. Rev. A **14**, 608 (1976).
[28]J. T. Park, J. E. Aldag, J. M. George, J. L. Peacher, and J. H. McGuire, Phys. Rev. A **15**, 508 (1977).
[29]J. George, Ph.D. dissertation, University of Missouri—Rolla, 1978.
[30]J. Aldag, Ph.D. dissertation, University of Missouri—Rolla, 1980.
[31]J. T. Park, IEEE Trans. Nucl. Sci. **NS25**, 1011 (1979).
[32]J. E. Aldag, J. L. Peacher, P. J. Martin, V. Sutcliffe, J. George, E. Redd, T. J. Kvale, D. M. Blankenship, and J. T. Park, Phys. Rev. A **23**, 1062 (1981).
[33]John T. Park and F. D. Schowengerdt, Rev. Sci. Instrum. **40**, 753 (1969).
[34]E. Redd and J. T. Park, Rev. Sci. Instrum. **55**, 119 (1984).
[35]C. E. Kuyatt and E. W. Plummer, Rev. Sci. Instrum. **43**, 108 (1972).
[36]C. E. Kuyatt (private communication).
[37]J. Arol Simpson, Rev. Sci. Instrum. **35**, 1698 (1964).
[38]C. E. Kuyatt and J. Arol Simpson, Rev. Sci. Instrum. **38**, 103 (1967).
[39]H. Hafner, J. Arol Simpson, and C. E. Kuyatt, Rev. Sci. Instrum. **39**, 33 (1968).
[40]*Atomic Energy Levels and Grotrian Diagrams 1: Hydrogen I—Phosphorus XV,* edited by Stanley Bashkin and John O. Stoner, Jr. (North-Holland, Amsterdam, 1975).
[41]J. T. Park, *Collisional Excitation of Simple Systems,* in *Collisional Spectroscopy,* edited by R. G. Cooks (Plenum, New York, 1978).
[42]*Atomic Data for Controlled Fusion Research,* edited by C. F. Barnett, J. A. Ricci, M. I. Wilker, E. W. McDaniel, E. W. Thomas, and H. B. Gilbody (Oak Ridge National Laboratory, Oak Ridge, 1977).
[43]D. R. Schoonover and J. T. Park, Phys. Rev. A **3**, 228 (1971).
[44]Thomas Richard McCalla, *Introduction to Numerical Methods and FORTRAN Programming* (Wiley, New York, 1977).
[45]J. T. Park, Adv. At. Mol. Phys. **19**, 67 (1983).
[46]Cosntantine E. Theodosiou, Phys. Rev. A **22**, 2556 (1980).
[47]J. B. Delos, Rev. Mod. Phys. **19**, 67 (1983).
[48]M. Kimura and W. R. Thorson, Phys. Rev. A **24**, 1780 (1980).